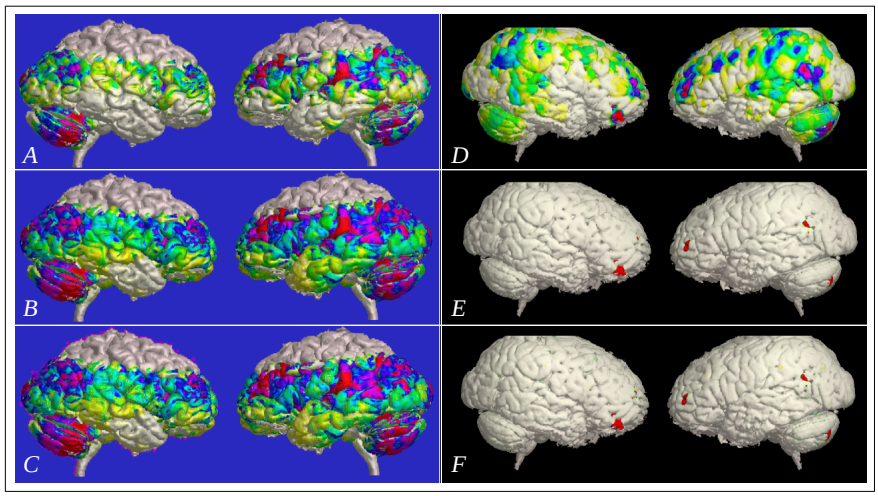

Figure 5.6 *Normal Fusion renderings of the right and left hemisphere using the maximum value of a functional dataset over a depth range of 0–10 mm to color encode the corresponding surface voxel extracted from MRI data. Frame (A): Surface color encoding of FDG–PET activity for an epileptic patient. Frame (B) is the result of color manipulation of Frame (A) via the separate storage scheme, Frame (C) is the result with the recalculation scheme. Frame (D): Surface color encoding of HMPAO–SPECT for a patient with TS. Frame (E) is the result via the separate storage scheme, Frame (F) with the recalculation scheme. The lookup table is shown in Figure 5.3B.*

The stimulation was evoked by a simple finger opposition task with the right hand by a right-handed subject. The task entailed repeatedly and sequentially touching the thumb once with each one of the digits. A total of eight PET and eight MRI datasets (four stimulus and four non-stimulus sets) were acquired and processed as identical as possible to properly compare both functional modalities. Statistical analysis utilized standardized normal variates based on repeated measurements within a single subject, referred to as a z_t-map (for details we refer to (Van Gelderen et al. 1995)). Both an fMRI and a PET z_t-map were calculated to denote the difference in, *resp.* fMRI and PET activity between activated and non-activated data. Furthermore, the PET data were resampled to the fMRI resolution, and the lookup tables of the integrated visualizations of both PET and fMRI had to be identical because both z_t-maps were statistically processed in order to have identical levels of activation.

MRI scans were obtained with a clinical 1.5 Tesla scanner (SIGNA, General Electric). The fMRI data were acquired with a 3D PRESTO sequence (Van Gelderen et al. 1995) (TE=35 ms, TR=24 ms, flip angle 11 degrees, slab thickness 65 mm with 90 mm FOV, data matrix $64 \times 50 \times 24$, 6.0 sec scan time, pixels of $3.75 \times 3.75 \times 3.75$ mm). For registration purposes an IR sequence (TI/TR 800/3000 ms, slice thickness of 2.75 mm, 1 mm gap, 24 slices spanning 90 mm, FOV 240 mm, 256×128, 7 min

scan time) was acquired which matched the fMRI data in both location and orientation. Anatomical images of the whole brain volume were acquired with a spoiled GRASS sequence (TE/TR 5.1/20 ms, 124 contiguous slices of 1.2 mm thickness, 300 mm FOV, 256×256) and used for localization and for registration purposes of all functional data. The $H_2{}^{15}O$ PET images were obtained with a Scanditronix brain tomograph (15 contiguous slices, 6-6.5 mm in-plane and axial resolution after reconstruction).

The results for PET/MRI and fMRI/MRI are shown in Figure 5.5. The hot-spots visible in both the PET/MRI and fMRI/MRI visualizations bear a high resemblance in size and activity. Furthermore, the hot-spots are both located in the section of the PSM area corresponding with the finger opposition stimulus.

On the 2D image slices, the hot-spots could be easily recognized for this case, but the anatomical localization requires mental integration of the functional with the anatomical data. Also, the pattern of gyri and sulci is hard to follow when using 2D slices only. The Normal Fusion visualizations assist in establishing the relationship of the functional information to the anatomy.

5.3.2 PET/MRI brain images of epilepsy

This case reports on a patient diagnosed with an epileptic focus in the right hippocampus. FDG–PET was used as a metabolic tracer to acquire functional information. The Normal Fusion procedure was applied to display the metabolic effects of the epileptic focus on the cortex.

The FDG–PET data were acquired in the inter-ictal state with a 951 CTI/Siemens tomograph. A total of 31 contiguous transaxial planes parallel to the long axis of the temporal lobe were acquired, 5 mm in thickness, with a 3.4 mm slice separation (center to center) simultaneously covering 11 cm of axial FOV. A 3D T1-weighted gradient-echo MR image was acquired with 140 1.2 mm contiguous axial slices, TR=30 ms, TE=13 ms, 256×256 matrix, and 230 mm FOV of the head with a whole-body Philips Gyroscan 0.5 Tesla.

The results for FDG–PET (see Figure 5.6*A*) are suggestive of; *i)* an atrofic right temporal lobe, and *ii)* decreased PET activity in the frontotemporo-parietal area. From this image it is not clear whether the right temporal lobe is hypometabolic compared to the left temporal lobe.

5.3.3 SPECT/MRI brain images of the Gilles de la Tourette syndrome

The image data presented in this subsection concern a seven year old right-handed patient diagnosed with TS (see also Figure 4.2 for Normal Fusion images color encoded with a lookup table resembling a reversed heated-object scale).

Information on brain anatomy was acquired from a T1-weighted 3D gradient-echo MR image (127 1.3 mm contiguous axial slices with TR=30 ms, TE=13 ms,

256×256 matrix, and 230 mm FOV of the whole head with a whole-body Philips Gyroscan 0.5 Tesla). Information on cerebral blood perfusion was obtained from a HMPAO–SPECT scan acquired with a Picker PRISM^r three-detector gamma camera and reconstructed to 44 slices with a 64×64 matrix, a slice thickness of approximately 7.1 mm, and a plane resolution of 7.5 mm FWHM.

The integrated display shown in Figure 5.6*D* is the result of the Normal Fusion procedure applied to the SPECT/MRI datasets. The top of the brain was not scanned. Several differences can be noted when comparing the left and right hemisphere, *viz.*; *i)* a hot-spot in the right lateral fronto-orbital region, *ii)* increased activity in the left dorsal parietal lobe, and *iii)* increased activity in the left dorsal cerebellum, with a normal right cerebellum. It is not clear from this image what the level of activity is in the right lateral fronto-orbital hot-spot compared to the rest of the visualized cortical activity.

5.3.4 Retrospective color manipulation

The two cases depicted in Figure 5.6 illustrate the effects of interactive color manipulation. Initial examination of the PET/MRI Normal Fusion results suggested an atrophic left temporal lobe (Figure 5.6). Whether the metabolic activity of this temporal lobe was abnormal could not be discerned from this image. Manipulation of the color encoding using the HSV scheme (see Figures 5.6*B* and *C*) allowed rapid appreciation of the functional information; indeed the left temporal lobe had a lower metabolic activity when compared to other cortical regions. With the SPECT/MRI TS case, it proved of interest to refer the activity of the right lateral fronto-orbital hot-spot to activity in other cortical regions. Manipulation of the color encoding (see Figures 5.6*E* and *F*) rapidly showed that the fronto-orbital hot-spot was the most prominent of the visualized cortical regions.

The two strategies that were tested have both advantages and disadvantages. The first strategy, separate storage (see Figure 5.6*B* and *E*) requires only a simple tool, no limitations are set for the lookup table, and it is precise; but unfortunately, dedicated software is required for presentation. The second strategy, recalculation (see Figures 5.6*C* and *F*), introduces artefacts when using interpolating rendering algorithms. These artefacts are best noted in the border pixels of the object in Figure 5.6*C*. Changing the background color during rendering to a color not present in the HSV lookup table, *e.g.*, black, solves the artefacts at the border pixels (see Figure 5.6*F*). Furthermore with recalculation, the lookup table has to follow several limitations and it requires a more intricate tool than with separate storage. On the other hand, recalculation has the major advantage that all the required information can be stored and presented in any image format that support 24-bit images, such as TIFF and PNG.

5.4 Results II: Clinical evaluation

Already during the test trials setting up the evaluation of the color manipulation, observations were so obvious in favor of the color manipulation technique that we decided to skip the actual validation. The nuclear medicine physicians immediately considered color manipulation an asset because interpretation of the functio-anatomical images, and functional images in general, tends to rely on several steps with each an optimal color encoding. This calls for multiple color encoded images or color manipulation. For instance, correlation of functional information to a reference area like the cerebellum requires a different color encoding than localization of a hot-spot or detection of patterns of functional activity. Also, high activity present in extracranial tissue, *e.g.*, the salivary glands, or markers may seriously interfere with the determination of a proper lookup table.

The experiments with the 30 SPECT/MRI cases revealed that the proposed lookup table required little or no training. The approach to couple an additional function to a mouse button for manipulation of several control points at once (see Section 5.2.6) was well appreciated by the nuclear medicine physicians.

5.5 General discussion

Both the proposed Normal Projection technique and the color encoding scheme are simple to implement. The color mapping tables can be characterized by just a few control points since piece-wise linear hue and saturation assignment schemes give good results and a graphical user interface for the color manipulation is straightforward, both in VROOM and as a stand-alone program. Also, the histogram of the functional information in the brain can be calculated for an initial guess of the control points of the graph. We used percentages of the area under the graph, *e.g.*, 80%, 90%, 95%, and 100% for control points A, B, C, and Max. Overall, the approach does not require a new rendering each time the color encoding is changed. This not only allows rapid manipulation since the image manipulation is basically 2D processing, but it also requires little storage especially when compared to the original datasets.

In practice, observers tend to have different preferences with respect to color encoding and manipulation. This is caused by personal characteristics such as experience, training, the task, perceptual (dis-)abilities, but also by environmental factors such as the monitor and lighting conditions. The variation between humans in their color discrimination capability is considerable (Murch 1984c). Color display is one of those fields where one observer's dream can be another observer's nightmare. From the clinical evaluation it was clear that this problem can probably be tackled best by supplying an observer with the ability to chose the color encoding and manipulate the lookup table in an easy fashion.

A fair fraction (9%) of the male population is color blind (Gouras 1991). However, only a fraction of these are monochromatic or truly color blind (Murch 1984c).

The dichromats confuse only a small fraction of possible color pairs and can differentiate most color pairs at all relative brightnesses (Livingstone and Hubel 1988). This implies that careful choice of the lookup table and subsequent manipulation may well circumvent the impoverished color vision.

When we compared the results obtained with the normal direction and the viewing direction (see (Levin et al. 1989) and Chapter 4), we observed that color and shape both contribute to the delineation of structures like gyri and sulci (see also (Livingstone and Hubel 1988)). However, color can also seriously camouflage the anatomical information of the brain surface as was most noticeable with the use of the viewing direction where colors are painted over sulci (see also (Christ 1975) on subject's accuracy in identifying achromatic target features when adding colors to the display). Integration of information along the inward normal direction presented images where color and shape strengthened one another. The additional manipulation of the color encoding effectively counteracts any remaining camouflaging effects.

The use of chromatic information for attention and achromatic information for the surface of the brain apparently exploits the different pathways of the visual system quite efficiently. The human visual system appears to process grey and color independently and they only combine at a high level in the perceptual hierarchy. Entirely separate channels are thought to handle distinct parts of the visual information where three parallel pathways process information for motion and depth, form, and color separately. The parvocellular interblob system is thought to specialize in high-resolution form perception, the parvocellular blob system specializes in color, and the magnocellular system is specialized in motion and spatial relationships. The automatic interpretation of a 2D image into 3D information seems to be performed only in the achromatic magno system, not in the parvo system. For an extensive overview we refer to (Livingstone and Hubel 1988, Gouras 1991, Kandel 1991). One important aspect is not used in our technique, *i.e.*, the magnocellular system is also specialized in motion and this may provide a natural extension to use as a next item for the improvement of interpretation of the integrated medical images.

We have demonstrated that our approach is an important asset in the investigation of data from multiple modalities. The clinician can be supplied with several renderings of the multimodal volume data from well-chosen viewpoints over different depths (see also Chapter 4) with dedicated software for manipulating the color encoding. This offers the clinician a powerful tool for investigation and communication (with, *e.g.*, a radiologist or the referring clinician) of the functional data of the surface layer of the brain in relation to the anatomy, without the need for the original data and the rendering software.

Although we only present examples for the brain, the Normal Fusion technique extends to applications with other anatomical surfaces, *e.g.*, heart, liver, and bone. An example can be found in (Zuiderveld et al. 1995), where the technique is applied to calculate and visualize the thickness of the skull. The HSV color encoding approach also extends to other 3D multimodality visualization techniques such as the

multimodal cutplane (Payne and Toga 1990) (Chapter 3) or for display of information from time series like EEG, MEG, or perfusion CT or MRI.

5.6 Conclusions

We have applied the HSV color model with the Normal Fusion technique for integrated visualization of anatomical surfaces and functional data. The Normal Fusion technique is independent of the viewing direction and accurate in anatomical localization, because it follows the curvature of the surface (here: brain) to calculate the regional quantitative information (here: activity of cortical cells). Fusion of the calculated activity with the information from the rendering is based on the HSV color model; hue and saturation are used for the functional information, value for the rendering information. This allows easy, rapid, and intuitive retrospective manipulation of the color encoding of the integrated visualization. Experimental evidence is presented that the integrated display enhances appreciation of functional data of the surface layer of cortical grey matter within an anatomical frame of reference from MRI.

Acknowledgements

We are indebted to our colleagues W.F.C. Baaré, R. Debets, J.K. Buitelaar, B. Sadzot, N.F. Ramsey, H.E. Hulshoff Pol, J.H. de Groot, A.W.L.C. Huiskes, J.W. van Isselt, R. Jonk, J.M.H. de Klerk, J.B.A. Maintz, L.C. Meiners, I.J.R. Mertens, M. Metselaar, P.P. van Rijk, G.R. Timmens, and T. van Walsum for their contributions. We gratefully acknowledge the research licence of ANALYZE^{TM}, provided by Dr R.A. Robb, Mayo Foundation/ Clinic, Rochester, Minnesota.